THE CHARACTERIZATION OF WIDESPREAD FATIGUE DAMAGE IN FUSELAGE STRUCTURE

113056

N95-19472

Robert S. Piascik
NASA Langley Research Center
Hampton, VA

Scott A. Willard
Lockheed Engineering and Science Company
Hampton, VA

Matthew Miller
Boeing Commercial Airplane Group
Seattle, WA

ABSTRACT

The characteristics of widespread fatigue damage (WSFD) in fuselage riveted structure were established by detailed nondestructive and destructive examinations of fatigue damage contained in a full size fuselage test article. The objectives of this work were to establish an experimental data base for validating emerging WSFD analytical prediction methodology and to identify first order effects that contribute to fatigue crack initiation and growth.

Detailed examinations were performed on a test panel containing four bays of a riveted lap splice joint. The panel was removed from a full scale fuselage test article after receiving 60,000 full pressurization cycles. The results of *in situ* examinations document the progression of fuselage skin fatigue crack growth through crack linkup. Detailed tear down examinations and fractography of the lap splice joint region revealed fatigue crack initiation sites, crack morphology and crack linkup geometry. From this large data base, distributions of crack size and locations are presented and discussions of operative damage mechanisms are offered.

INTRODUCTION

The incidence of airframe fatigue damage increases as airplanes are operated past their economic design objective, typically 20,000 flights. Because of reduced durability and related safety concerns, the commercial aircraft industry has instituted elaborate inspection and maintenance requirements to ensure continued airworthiness of aging airplanes. As part of industry's initiative to ensure safe operation of aging commercial aircraft, pressure testing of full scale fuselage structure is conducted to simulate flight loads [1-4]. Detailed structural examinations performed during the full pressurization tests often lead to design improvements and practical inspection programs. The airframe industry has entered into a cooperative aging aircraft program with NASA Langley Research Center (LaRC) to resolve durability issues associated with the aging commercial airplane fleet. As part of this cooperative effort, LaRC has performed detailed examinations of commercial aircraft structure that has been subjected to long term pressure tests. The objectives of these examinations are two fold: (1) Develop an understanding of widespread fatigue damage (WSFD) in fuselage lap splice joint structure, characterize crack initiation, growth and link-up, and (2) Use the knowledge gained here to benchmark critical laboratory simulations, analytical predictions and advanced nondestructive inspection techniques. Described herein are the results of detailed teardown examinations performed on a fuselage skin lap splice joint containing widespread fatigue damage.

BACKGROUND

Full scale testing of a fuselage structure was conducted to demonstrate structural airworthiness to 60,000 full pressure (0 to 9.0 psi) cycles, i.e., three times the minimum economic design objective [1]. Details of the fuselage structure and test conditions are described in reference 1. During pressure testing, *in situ* inspections were performed to develop a detailed understanding of fuselage durability. Cracks in the fuselage skin lap splice joint were observed in a few localized regions of the structure. The lap splice joint is formed by overlapping and joining two sections of fuselage skin (Alclad 2024-T3) using a four row riveted (Briles design) construction. Each bay is separated by a bonded and riveted

tear strap identified by the vertical dashed lines in Figure 1. The function of the tear strap is to act as a fail safe load path and a crack arrest feature. A horizontal frame (stiffener), not shown in Figure 1, is riveted (third row from the top) along the length of the lap splice joint inner surface. A sealant is applied to the lap splice mating surfaces to prevent internal pressure loss during flight and to inhibit joint corrosion.

Figure 1 is a schematic of bay #1 summarizing the results of *in situ* visual examinations conducted during fuselage pressure testing. After 20,000 pressure cycles, inspections were conducted at intervals of approximately 1700 cycles. The small arrows in Figure 1 mark the upper row rivet locations that contained visible cracks. The first evidence of cracking was observed near the mid-bay after 38,333 cycles. No further cracking was observed in bay #1 until 50,250 pressurizations, when three mid-bay cracks were noted. At 55,500 cycles, ten rivet locations contained cracks. The first evidence of crack link-up was observed after 58,200 cycles. An additional 1800 pressurizations were performed, totaling 60,000 cycles, before cracks at all upper row rivet locations had linked-up. A single long crack, 47.9 cm (18.85 inch) in length, had formed along the upper row of rivets, terminating at the adjacent tear straps. After completing the three lifetime test, the four bay region containing wide spread fatigue damage was removed for detailed teardown inspection at LaRC. Upon completion of pressure testing and in situ inspections, a four bay panel of lap splice joint containing WSFD was removed from the fuselage test article for a detailed teardown inspection at LaRC. Reported herein are the results of examinations conducted on one (bay #1) of the bays from that four-bay panel.

LaRC INSPECTION RESULTS

Non-destructive Examinations (NDE)

Prior to destructive examination, bay #1 was examined visually (10X) and by eddy current techniques. These laboratory inspections yielded results similar to that obtained by *in situ* examination. With one exception, all outer skin fatigue cracks were observed in the upper row rivet locations shown in Figure 1. The single exception was observed in the most

forward rivet of the second row. The location and description of this outer skin crack was confirmed later by the destructive examination. Subsurface or inner skin fatigue cracking was not detected by NDE. Figure 2 is a photograph showing the long outer skin crack located along the upper row of rivets in bay #1. Figure 2b details the link-up crack path for fatigue cracks propagating from rivets 5, 6, and 7. Interacting "curved" cracks shown in Figure 2b have been observed in the laboratory and modeled by Ingraffea et al. [5].

The following is a summary of observations from the bay #1 lap splice joint nondestructive examinations.

1. Through-thickness outer skin cracking is primarily contained along the upper row of rivets.
2. All upper row fatigue cracks initiated at the rivet hole horizontal centerline or in the upper half of the hole. The crack propagated nearly normal to the fuselage hoop stress. A curved crack path in middle bay regions, noted in Figure 2, occurred as a result of crack interactions during link-up. Crack link-up of long to short cracks at the outer extremities of the bay exhibited less curvature. The long upper row crack was somewhat deflected by both tear straps; a slight upward crack path was noted at each end of the bay.
3. The upper surface of the long crack was displaced outward, "pillowed". Here, the outer skin was no longer captured by the rivet head. This observation and destructive examination results, discussed later, suggest Mode III displacements had occurred after crack link-up between many rivets, possibly 8 to 10 rivet lengths. Presumably, at long crack lengths, the outer skin can no longer be restrained by the rivet heads and forces due to internal pressure resulted in pronounced out-of-plane displacements. This Mode III effect has been studied by Hui and Zehnder [6].
4. Examination of bay #1 inner surfaces revealed no evidence of cracking.

Destructive Examinations

Destructive examinations were performed to characterize wide spread fatigue cracking in lap splice fuselage structure. Special care was taken when dismantling the bay #1 lap splice joint to maintain traceability and to eliminate possible extraneous damage and/or contamination. The entire upper row of rivets containing the long crack was removed intact by making a horizontal cut slightly below the upper row. This allowed the removal and subsequent examination of the long crack fracture surface without disturbing the remainder of the bay. Each of the remaining 52 rivet locations contained in the lower three rows were individually removed from the panel as illustrated in Figure 3. After each rivet location was removed, the rivet was sectioned from top to bottom, using a slow speed diamond saw, exposing the aft and forward sections of the rivet hole. Each rivet half was removed with little or no force, thus exposing the hole inside diameter without disturbing the surface. To open small incipient fatigue cracks located on the rivet hole surface, each specimen (a total of 102 specimens) was strained in a three point bend fixture depicted in Figure 3. All rivet hole surfaces were examined in detail using both optical and scanning electron microscopy (SEM). Typically, each specimen was examined three times. The hole surface was examined twice after partial straining operation; the location of small partially opened incipient cracks were charted after each straining operations. A third detailed fractographic examination was performed after final fracture of the specimen which typically exposed the major fatigue crack.

Fatigue Crack Location

Figure 4 summarizes the results of the destructive examination. Figure 4a is a schematic of bay #1 identifying the four rows of rivets (rows G, H, I and J), the location of the long crack along row J and the location of smaller cracks found in rows G, H and I during the destructive examination. Figures 4b, 4c and 4d are schematics (not drawn to scale) of each rivet row detailing the location, initiation site (arrow) and length of each fatigue crack. Crack depth was computed from the point of initiation to the point of greatest crack depth (length) or, for through-thickness cracks, from the rivet hole surface to the point

of greatest crack depth. In rows G, H and I, 17 holes of the 52 examined were found to contain fatigue cracks. A total of 23 fatigue cracks were found in rows G, H and I. Row I contained six outer skin cracks; the crack located at hole position "0" was detected by eddy current inspection. All other fatigue cracks in row I were small and located under the rivet head. Row H contained four inner skin fatigue cracks, two through-thickness cracks located at positions 17 and 18 and small cracks at positions 4 and 15. Row G exhibited cracking in eight rivet holes. Hole locations 13 and 14 contained through-thickness fatigue cracks. The remaining six holes contained smaller surface and corner cracks. The site of crack initiation varied; Row I contained outer skin cracking that primarily initiated along the mating surface between the outer and inner skin, Row H contained inner skin cracks that initiated at rivet hole corners, rivet hole surface and outer/inner skin surface, and Row G contained cracks that initiated at rivet hole corners, rivet hole surfaces and outer/inner skin surface.

Fatigue Crack Morphology

The SEM micrographs shown in Figure 5 illustrate the typical transgranular morphology and location of fatigue cracks observed in the outer and inner skin of bay #1. Outer skin countersink cracking, located in region b in Figure 5a, is shown in Figure 5b. Typically, countersink cracks initiate at the inboard corner of the rivet hole marked by the arrow in Figure 5b. Here, the inboard corner of the countersink exhibits disturbed metal and possible evidence of local clad thinning. The outer skin surface cracks, shown in Figure 5c, initiate at surface clad discontinuities marked by the arrow. These surface cracks are located at the outer/inner skin interface near the rivet hole countersink identified by region c in Figure 5a. Evidence of surface clad abrasion (fretting) was observed at the point of crack initiation, i.e., clad surface disturbed metal, black oxide debris at the outer/inner skin interface and secondary microcracks at the clad metal interface in some cases. Rivet hole surface cracks, region d in Figure 5a, typically initiate at surface discontinuities identified by the arrow (fig. 5d). Inner skin corner cracks, located at region e in Figure 5a, initiate at corner discontinuities identified by the arrow in Figure 5e.

Detailed examination of the fracture surface from the long crack contained in upper row J (Figure 4a) revealed that outer-skin fatigue cracks initiated along the lap splice joint interface, identical to that shown in Figure 5c. Further examination of the fatigue fracture surfaces from each rivet hole revealed a thin region (ligament) exhibiting evidence of ductile tearing located along the outboard surface of the outer skin. Figure 6 shows the fracture morphology of upper row fatigue cracks at different stages of propagation from rivet holes located in adjacent bay #2. From Figures 6b, 6c and 6d, a pattern of fatigue crack propagation has been derived for the upper row locations and illustrated in Figure 6a. Figure 6d shows a third outer skin crack of approximately 3.8 mm (0.150 in) in length. Here, the subsurface crack had formed an outboard surface ligament similar to that observed in the upper row on bay #1. These results show that outer skin cracks initiate at the inner/outer skin interface (arrows in Figures 6b, 6c and 6d) and propagate in a subsurface manner depicted in Figure 6a.

Laboratory fatigue tests conducted at LaRC have confirmed that the fatigue crack morphology shown in Figure 6 is indicative of out-of-plane bending loads. Tension-bending (T/B) constant amplitude fatigue tests were conducted using 2.1 mm thick center-cracked alloy 2024T3 sheet specimens. The fatigue crack fracture morphology from a specimen tested at a T/B ratio of 1.5 is shown in Figure 7. Figure 7a is a SEM micrograph showing the fatigue crack front (dashed line) at region A in Figure 7b. The remaining ligament, shown in Figure 7a, exhibits a ductile tearing morphology produced when breaking the specimen by overload after fatigue testing. The fatigue crack/ligament morphology was formed on the compressively-loaded surface while substantial fatigue crack growth continued on the tension surface, thus forming a crack geometry similar to that observed along the lap splice upper row rivet holes.

Complex loading during fatigue cracking of the upper rivet row was also noted by scratches on the fracture surface oriented transverse to the direction of through-crack propagation. Presumably, out-of-plane motion of the upper portion of the fracture surface occurred at relatively long crack lengths, i.e., multiple fatigue crack link-up. This motion rubbed the mating fracture surfaces, forming the transverse scratches similar to that observed

by Zehnder and coworkers during Mode III testing of 2024-T3 sheet [7]. Based on fractographic analysis, significant out-of-plane (Mode III) motion is likely only when cracks are long and no longer captured by the rivet heads.

Lap Splice Joint Fretting

Upper rivet row fatigue cracking at the inner/outer skin interface shown in Figures 5c and 6 suggests that crack initiation is associated with localized damage due to fretting [8]. Evidence of fretting fatigue was noted by a black oxide deposit on the mating surface between the inner/outer skin around each rivet hole. Depicted in Figure 8 is the extent (area drawn to scale) of fretting debris (black oxide) observed on the inboard surface of bay #1 lap splice joint outer skin by estimating the area of fretting debris at each hole location. The amount of fretting was estimated by determining an arithmetic average of fretted surface area per the procedure shown in Figure 9. Here, a scaling factor was assigned to estimate the amount of fretting in each quadrant shown in Figure 9. The value 0 was assigned when no fretting was observed and 5 represented the highest degree of fretting. A "fretting Average" (FA) was calculated for each rivet position. A direct correlation of "fretting average" with rivet hole cracking was not conclusive, i.e., all fretting initiated cracks were observed in holes that exhibited a relatively high FA $>$ 3.00, but, all holes that exhibited a FA $>$ 3.00 did not contain fretting initiated cracks. Figure 10 is a plot of FA versus rivet hole location for the rows G, H, I and J. Here, a distinct correlation is observed for FA and rivet row, i.e., upper row J which contains the greatest number of fretting fatigue cracks, also exhibits the greatest evidence of fretting damage (highest FA level).

SUMMARY

The detailed destructive examination of bay #1 has shown that localized regions of fuselage lap splice joints do contain WSFD after 60,000 full cycle pressurizations. A summary of fatigue cracking contained in bay #1 is shown in Figure 11. Illustrated is the crack length distribution for the 53 fatigue cracks found in bay #1. The majority of cracks having lengths greater than 1.2 mm (30 of the 36 fatigue cracks) were contained in upper

row J. The majority of fatigue cracks observed in the remaining lower three rivet rows exhibited crack depths of less than 1.2 mm. Rows I and J, the two upper rivet rows, exhibited outer skin cracking. Only inner skin cracking was observed in lower rows G and H. Fatigue crack initiation occurs in regions of high K_T located at or near rivet holes. Typically, cracks were found to initiate at rivet hole corners, surface discontinuities (burrs, dents, etc.) and abraded (fretted) surfaces.

Results from fractographic analyses of upper row cracking suggested complex loading. Evidence of out-of-plane loading was suggested by subsurface fatigue crack propagation. In addition, increased Mode III displacement was evidenced by transverse rubbing of fatigue crack surfaces in regions where the outer skin bulging was no longer contained by the rivet head.

Evidence of fretting fatigue damage, black oxide debris, was noted at every rivet hole / lap splice interface in bay #1. Most fretting initiated fatigue cracks were contained in the upper row; here, all fatigue cracks initiated in the outer skin at the inner/outer skin interface in regions that exhibited increased surface abrasion (fretting damage).

ACKNOWLEDGEMENT

The contribution of Mr. E.P. Phillips is gratefully acknowledged. Mr. Phillips provided fatigue fracture surfaces from laboratory tension/bending tests.

REFERENCES

1. Gopinath K.V., Structural Airworthiness of Aging Boeing Jet Transports - 747 Fuselage Test Program, AIAA 92-1128, Feb. 1992.

2. Goranson, Ulf, G., and Miller, Matthew, Aging Jet Transport Structural Evaluation Programs, *Structural Integrity of Aging Airplanes*, Atlanta, GA, March 1990, Atluri, S.N., Sampath, S.N., and Tong, P., eds., Spinger-Verlag Berlin, 1991, pp. 131-140.

3. Hoggard, Amos, W., Fuselage Longitudinal Splice Design, *Structural Integrity of Aging Airplanes*, Atlanta, GA, March 1990, Atluri, S.N., Sampath, S.N., and Tong, P., eds., Spinger-Verlag Berlin, 1991, pp. 167-181.

4. Roll, R., van Dalan, A, and Jongebreur, A.A., Results of Review of Fokker F28

"Fellowship" Maintenance Program, *Structural Integrity of Aging Airplanes*, Atlanta, GA, March 1990, Atluri, S.N., Sampath, S.N., and Tong, P., eds., Spinger-Verlag Berlin, 1991, pp. 309-320.

5. Ingraffea, A.R., Grigoriu, M.D. and Swenson, D.V., Representation and Probability Issues in the Simulation of Multi-Site Damage, *Structural Integrity of Aging Airplanes*, Atlanta, GA, March 1990, Atluri, S.N., Sampath, S.N., and Tong, P., eds., Spinger-Verlag Berlin, 1991, pp. 183-197.

6. Hui, C.Y. and Zehnder, A.T., A Theory For The Fracture of Thin Plates Subjected to Bending and Twisting Moments, *Int. J. Fracture*, 61, 1993, pp. 211-229.

7. Zehnder, A.T., Communication, Dept. of Theoretical and Applied Mechanics, Cornell University, NY (1994).

8. Schijve, J., Multiple-Site-Damage Fatigue of Riveted Joints, *Durability of Metal Aircraft Structures*, Atluri, S.N., Harris, C.E., Hoggard, A., Miller, N., and Sampath, S.N., eds., Atlanta Tech. Pub., Atlanta, GA, 1992, pp. 2-27.

9. Hartman, A., Some Tests on the Effect of Fatigue Loading on the Friction in Riveted Light Alloy Specimens, Nat. Aerospace Lab., Amsterdam, The Netherlands, TN M.2088, 1961.

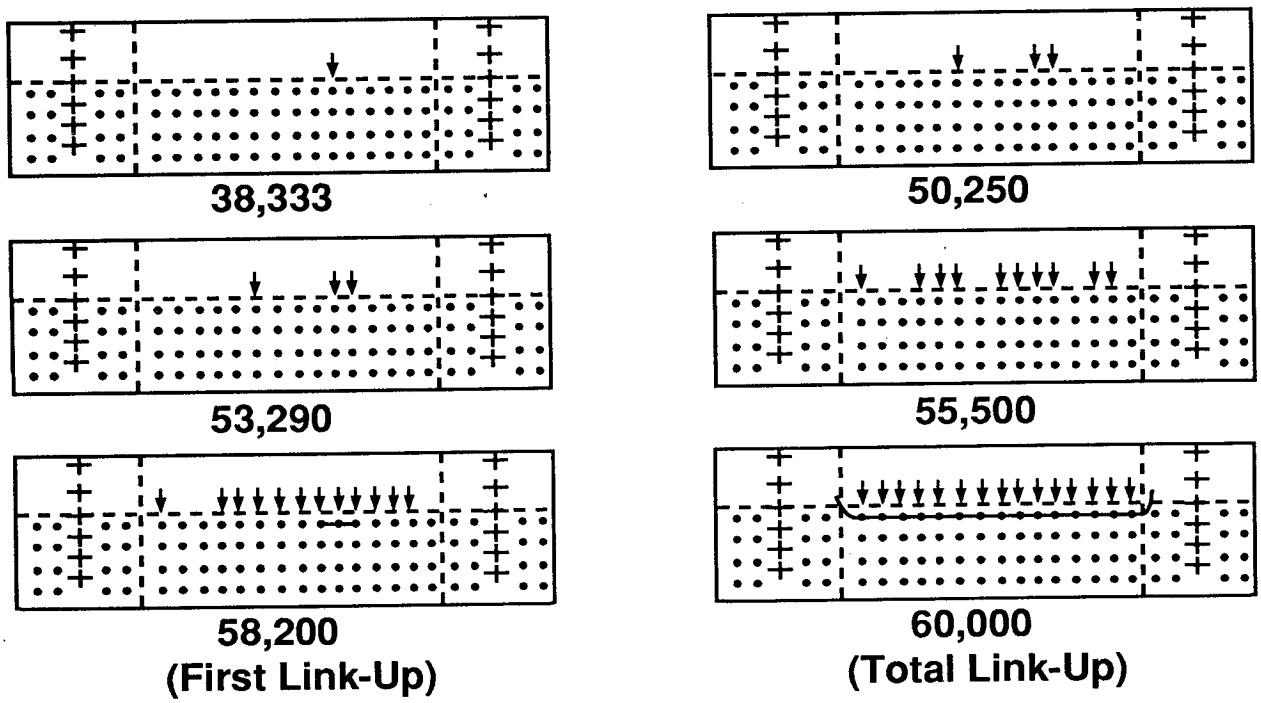

Figure 1. A schematic of bay #1 summarizing the location of outer skin fatigue cracks identified during visual in situ examinations.

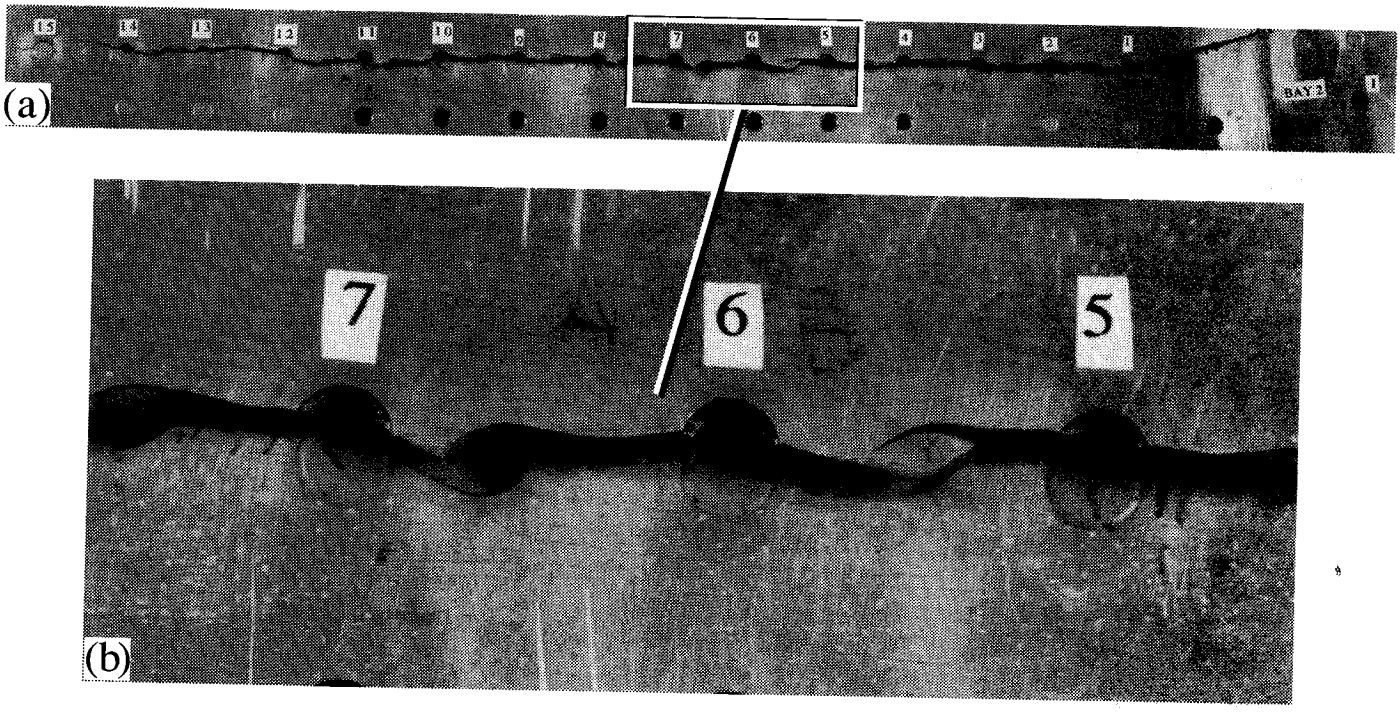

Figure 2. Photographs showing the fatigue cracking after link-up in bay #1 lap splice joint.

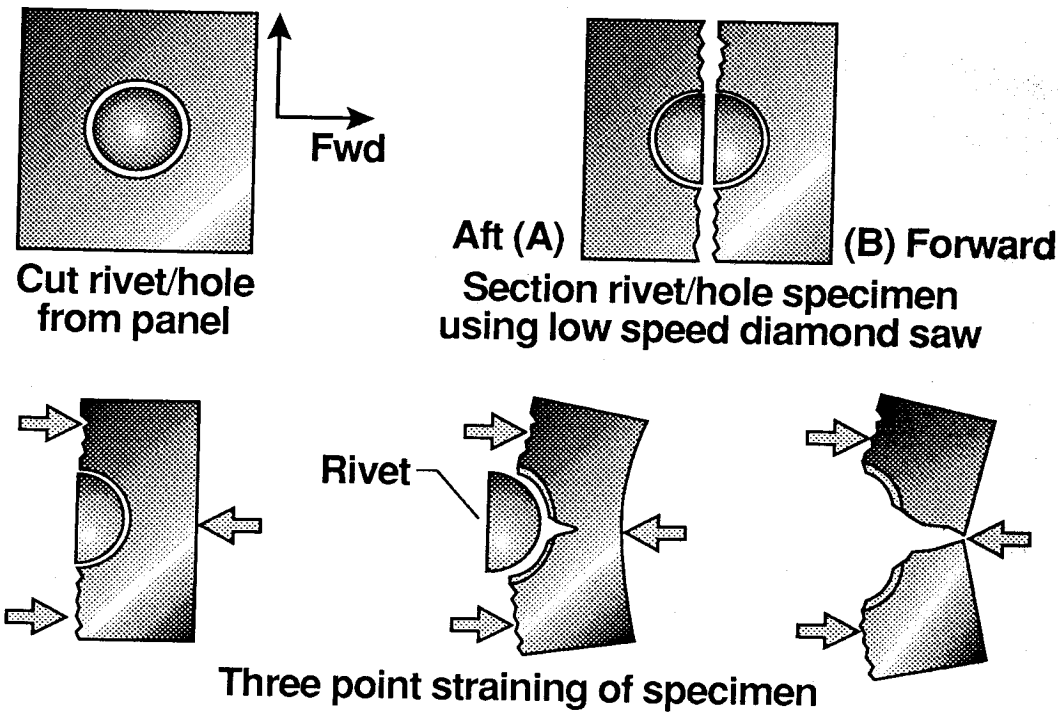

Figure 3. Schematic illustrating rivet hole destructive examination procedure.

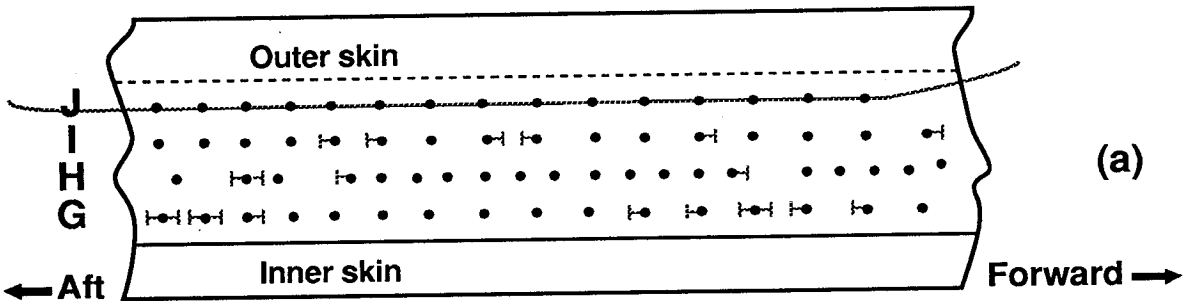

Row I

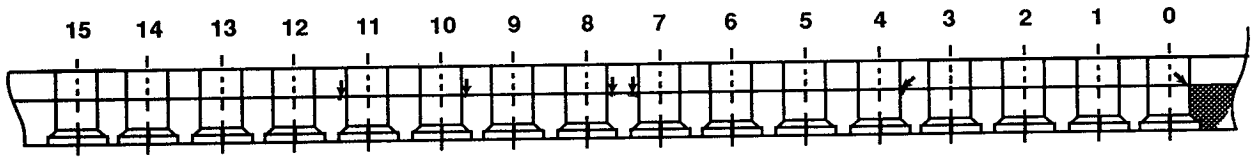

Hole #	Location	Length mm(in)	Hole #	Location	Length mm(in)
0 (FWD)	Outer skin	2.33 (.092)	8 (FWD)	Outer skin	0.073 (.003)
4 (FWD)	Outer skin	0.102 (.004)	10 (FWD)	Outer skin	0.140 (.006)
7 (Aft)	Outer skin	0.112 (.004)	11 (Aft)	Outer skin	0.058 (.002)

(b)

Row H

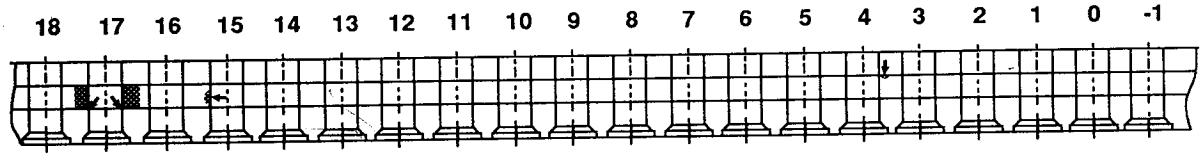

Hole #	Location	Length mm(in)	Hole #	Location	Length mm(in)
4 (FWD)	Inner skin	0.110 (.004)	17 (FWD)	Inner skin	3.51 (.138)
15 (Aft)	Inner skin	ND	17 (Aft)	Inner skin	4.00 (.157)

(c)

Row G

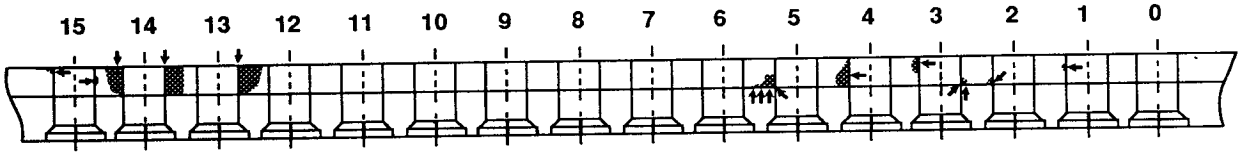

Hole #	Location	Length mm(in.)	Hole #	Location	Length mm(in.)
1 (Aft)	Inner skin	0.250 (.010)	13 (FWD)	Inner skin	2.750 (.108)
2 (Aft)	Inner skin	0.100 (.004)	14 (Aft)	Inner skin	2.720 (.107)
3 (1FWD)	Inner skin	0.170 (.007)	14 (FWD)	Inner skin	5.00 (.197)
3 (2FWD)	Inner skin	0.335 (.013)	15 (FWD)	Inner skin	0.163 (.006)
3 (Aft)	Inner skin	0.360 (.014)	15 (1-Aft)	Inner skin	0.115 (.004)
4 (Aft)	Inner skin	0.615 (.024)	15 (2-Aft)	Inner skin	0.128 (.005)
5 (Aft)	Inner skin	0.680 (.027)			

(d)

Figure 4. Illustrations showing the location of fatigue cracks in bay #1.

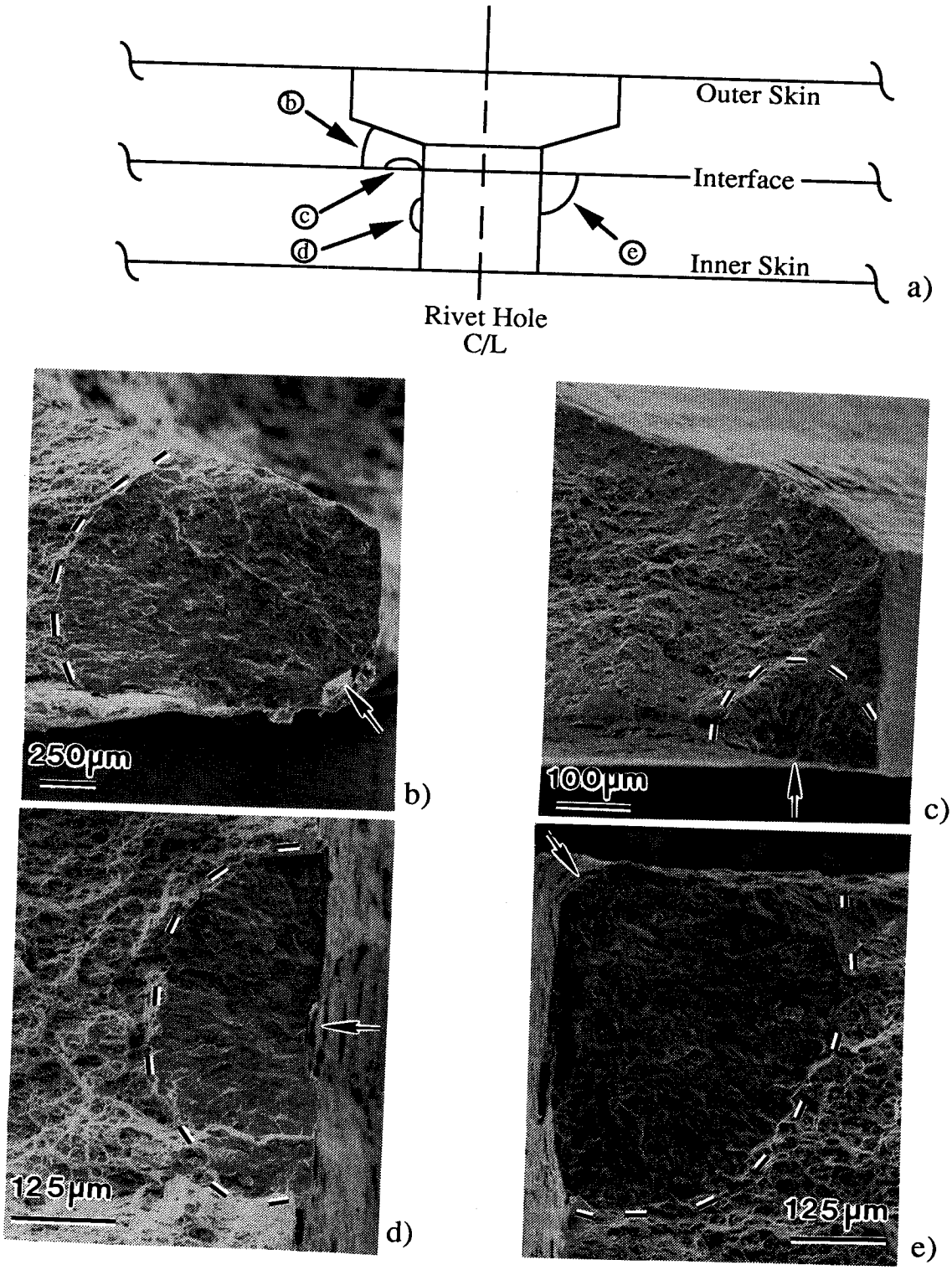

Figure 5. Schematic and SEM micrographs showing the location of fatigue cracking, crack initiation site (arrows) and fracture morphology of fatigue cracks in bay #1.

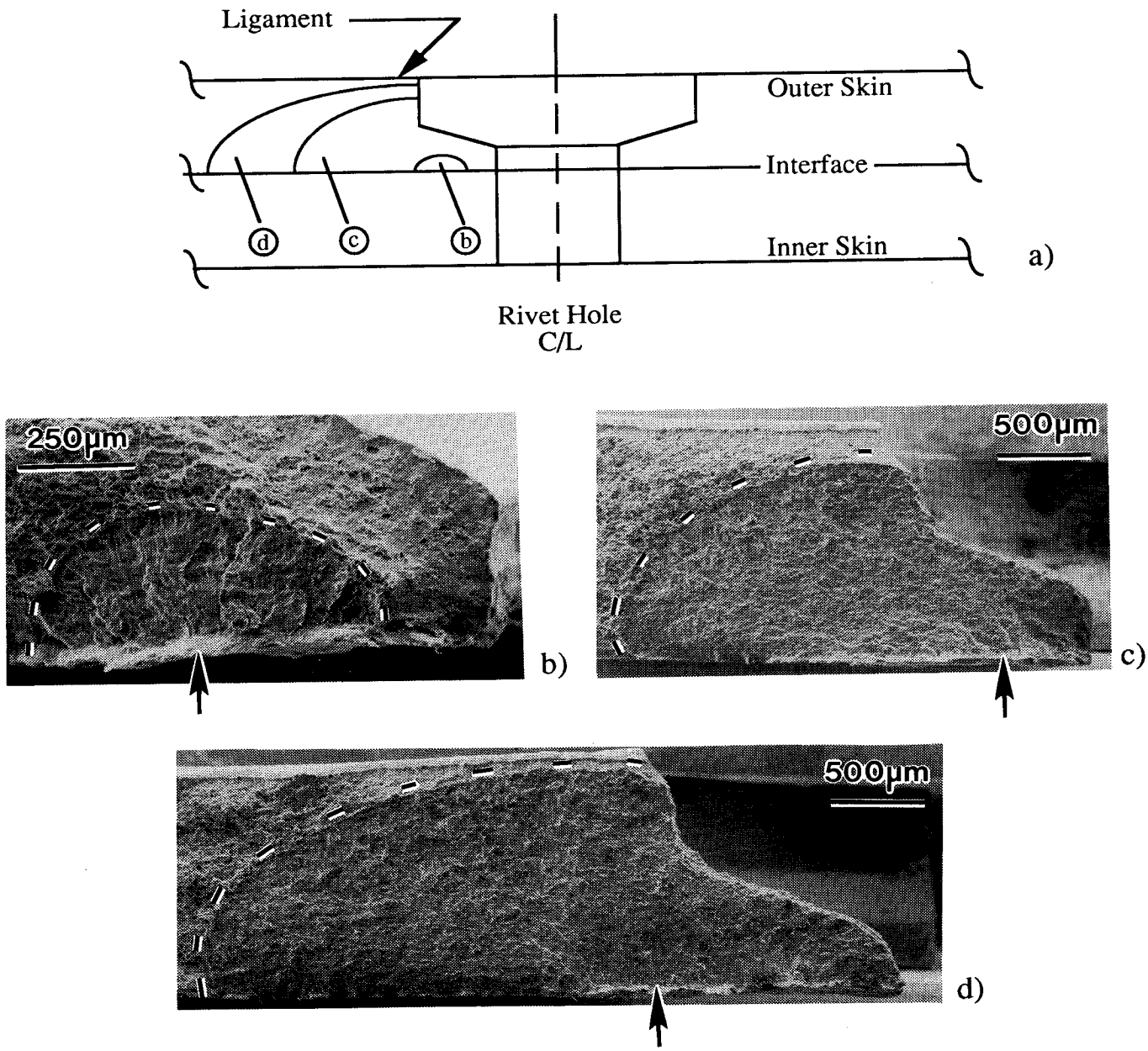

Figure 6. Schematic and SEM micrographs illustrating the location of fatigue crack initiation (arrows) and sequence of crack propagation in the lap splice upper rivet row.

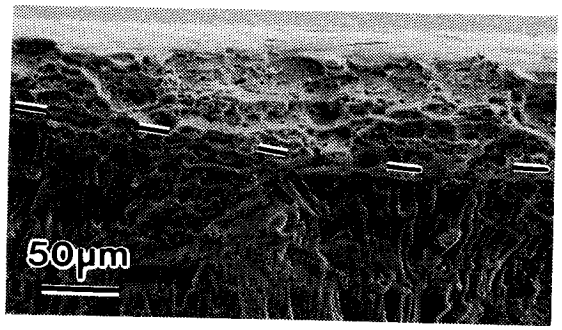

a)

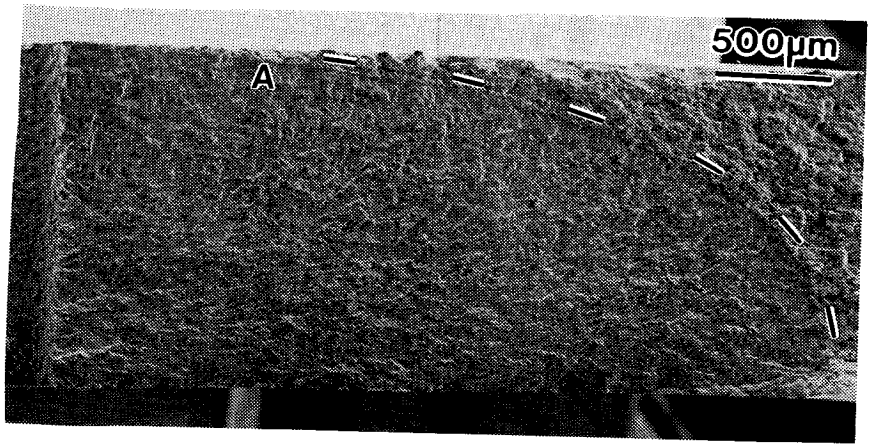

b)

Figure 7. SEM micrograph illustrating the fatigue crack path produced as a result of tension/bend constant amplitude testing.

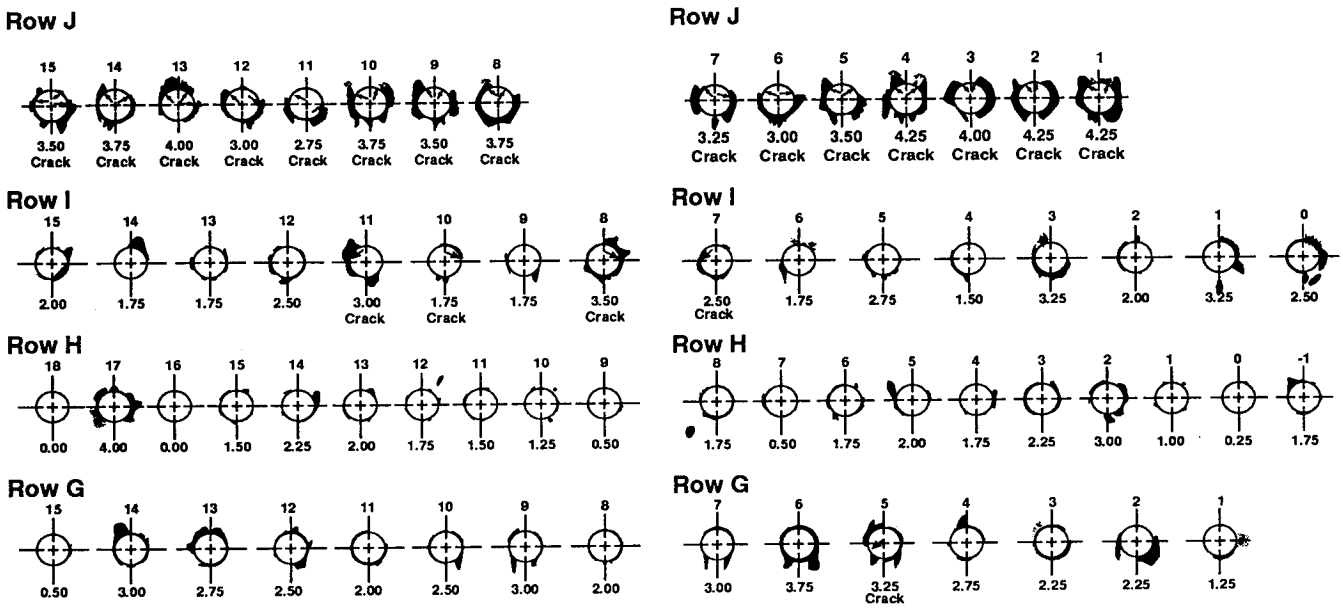

Figure 8. A schematic showing the interior surface of bay #1 lap splice outer skin. Illustrated is the location of black oxide film, the location of fretting intiated fatigue cracks and noted is the fretting average value determined by the procedure shown in Figure 9.

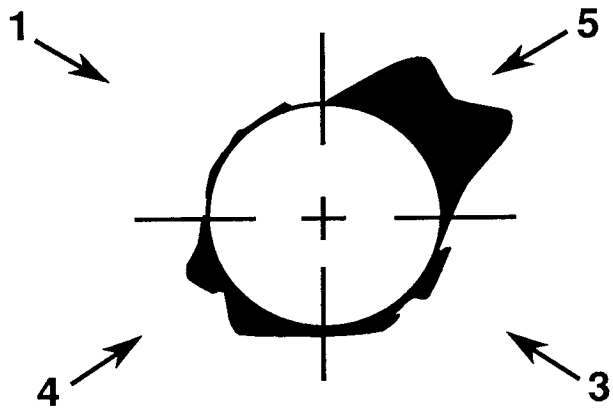

Fretting Average = (1+5+4+3)/4=3.25
Top Fretting Average = (1+5)/2=3.00
Bottom Fretting Average = (4+3)/2=3.50
LHS Fretting Average = (1+4)2=2.50
RHS Fretting Average = (5+3)/2 =4.00

Figure 9. A schematic showing the procedure used for estimating the extent of fretting fatigue by averaging the amount (area) of visual black oxide observed on the inside surface of the lap splice outer skin.

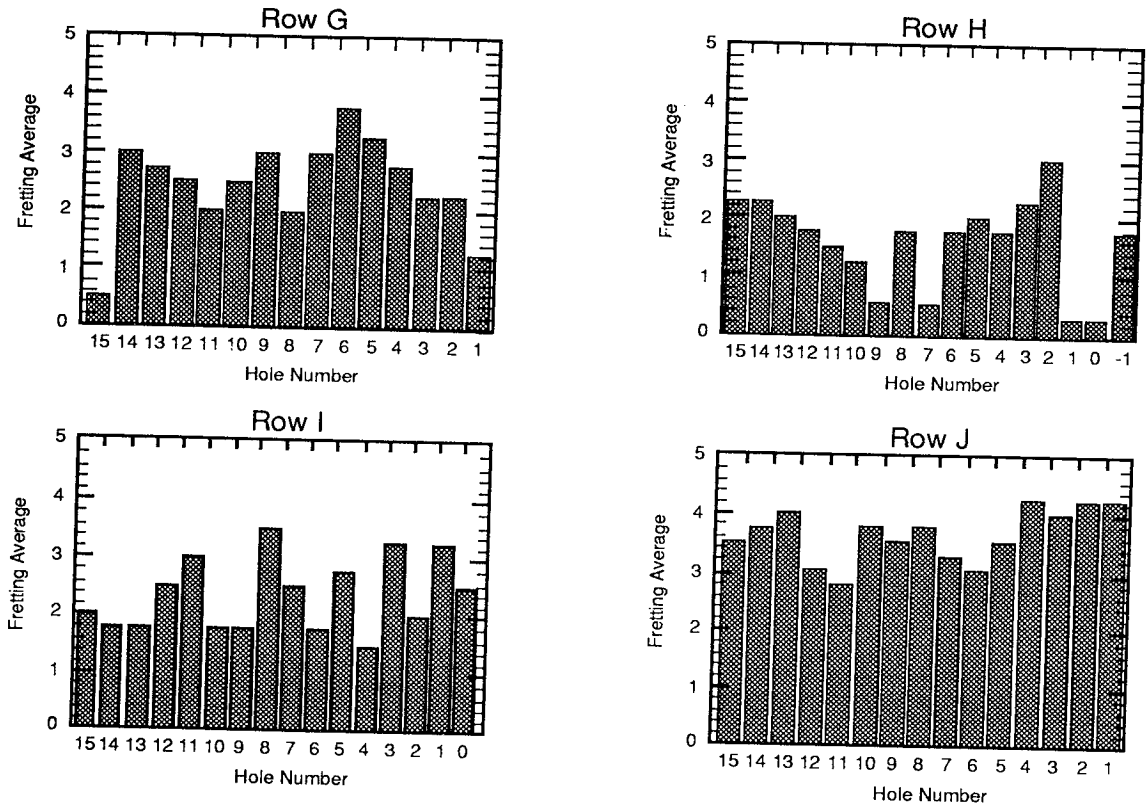

Figure 10. A plot of fretting average value versus rivet hole number is given for each rivet row (G, H, I and J) contained in bay #1.

Crack Length mm (x10^{-3}in.)	Number of Cracks Bay #1
0 to 1.19 (0 to 47)	17
1.2 to 2.39 (>47 to 94)	2
2.4 to 3.59 (> 94 to 141)	5
3.6 to 4.79 (>141 to 189)	6
4.8 to 5.99 (>189 to 236)	5
6.0 to 7.19 (>236 to 283)	5
7.2 to 8.39 (>283 to 330)	2
8.4 to 9.59 (>330 to 378)	0
9.6 to 10.79 (>378 to 424)	3
10.8 to 11.99 (>424 to 472)	2
12.0 to 13.19 (>472 to 519)	4
13.2 to 14.39 (>519 to 566)	1
14.4 to 15.59 (>566 to 614)	1
20.4 to 25.00 (>803 to 985)	0

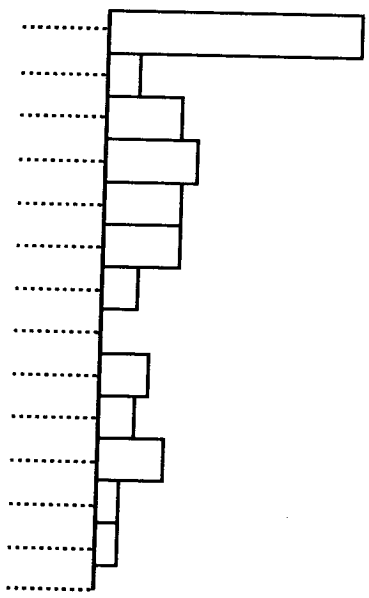

Figure 11. A plot showing the fatigue crack length distribution in bay # 1.